JMEPEG (2015) 24:2757–2763
DOI: 10.1007/s11665-015-1535-9

1059-9495/$19.00

Photocatalytic Activity of Immobilized Geometries of TiO_2

Hassan Koohestani and Sayed Khatiboleslam Sadrnezhaad

(Submitted September 18, 2014; in revised form April 14, 2015; published online May 7, 2015)

Photocatalysts that are used for waste water treatment are often suspended in the waste water during processing and then must be removed from the water after treatment. To reduce the post-degradation expenses and time, separation is facilitated by an immobilization process. The effect of immobilized TiO_2 geometries on the photocatalytic behavior of the photocatalyst is investigated in this work. Powder, fiber, film, and network-shaped TiO_2 nanocatalysts were produced by using different templates. The cellulose fiber and ceramic templates were used as substrates for fiber and film/network geometry production. The products were characterized by x-ray diffraction (XRD), scanning electron microscopy (SEM), and Brunauer-Emmett-Teller (BET) surface area measurement. The photocatalytic performance was determined by methyl orange degradation and cyanide photo-oxidation under ultraviolet irradiation. From the SEM images, the size range of the TiO_2 particles in the film and in the network geometries were 20-60 nm. The nanoparticles had covered the surface of the substrate, uniformly. Removal of the cellulose substrate by heat treatment yielded hollow TiO_2 fibers with diameters of 0.5-1 μm and lengths of 30 μm. The efficiencies of both photocatalytic reactions were obtained in the following order: powder > network > film > fiber geometry. The rate constant of the dye degradation reaction using powder catalyst was 0.0118 min^{-1}. For network catalyst, it was 0.0083 min^{-1}. Corresponding results for cyanide disinfection were 0.0055 and 0.0046 min^{-1}. Although powder samples had higher rate constants, network geometry was preferred due to its higher immobility.

Keywords cyanide, dye degradation, immobilized photocatalyst, micro-fiber, network structure

1. Introduction

Wastewater pollution has always been a major problem throughout the world. Suitable water used for drinking, agriculture, farming, etc., is declining through the years (Ref 1, 2). The water is gradually being contaminated with various pollutants such as inorganic and organic compounds. Metal processing due to urbanization and industrial activity is leading to water pollution by production of toxic metal ions existing in organic compounds. Because wastewater containing organic compounds leads to increased accumulation and biochemical oxygen demand, the water content decreases (Ref 3, 4). Appropriate methods of treating and water recycling are the key goals in preserving water resources (Ref 5).

Water treatment technologies such as adsorption or coagulation current cannot completely eliminate or destroy pollutions. Other conventional methods of water treatment such as sedimentation, filtration, ion exchange, etc., involve high operating costs and could generate toxic secondary pollutants into the ecosystem (Ref 5, 6).

In the past decades, numerous studies have been carried out by researchers from all over the world on the application of heterogeneous photocatalytic oxidation process to decompose and eliminate of water pollution (Ref 7).

Hassan Koohestani and **Sayed Khatiboleslam Sadrnezhaad**, Department of Materials Science and Engineering, Sharif University of Technology, Tehran, Iran. Contact e-mail: h_koohestani@mehr.sharif.ir.

Photocatalytic degradation of contaminants as a catalyst has been proposed as an advanced oxidation process (AOP) (Ref 8). AOP is based on the production of electron-hole pairs in the semiconductor by the absorption of ultraviolet (UV) radiation energy which is equal to or greater than the band gap energy. Among the various AOPs, TiO_2 heterogeneous photocatalysis has proven to be a promising technology for the decontamination of water pollution (Ref 9, 10).

Immobilizing photocatalysts can be effective in maintaining healthy water. It is important to produce stable photocatalysts which can be easily separated from clean water. This problem has resulted in development of several kinds of immobilization techniques to immobilize the TiO_2 powder, which may reduce the post-degradation expenses and time. In recent years, many researches have been done to produce different geometries of the photocatalysts and several structures were generated (Ref 11-13).

Catalyst particles should be separated from water by various methods to be reused for water treatment, because water containing these particles has a detrimental effect on living organisms (Ref 14). One way to make an immobile photocatalyst is to produce multi-dimensional structures such as thin film, nanotube, nanowire, fiber, network, etc., which is fixed to the walls of the water treating reactor (Ref 1, 15).

Of the various geometries, network structure, a hollow three-dimensional structure, has the potential for producing a new class of materials with novel applications. This structure is very important for practical applications because its pores have potentially large surface to volume ratio, which provide a significant advantage in the diffusion pathways that can be used as a kind of host for organic pollutants (Ref 15, 16).

In the present study, the effect of catalyst geometry, i.e., TiO_2 powder, fiber, film, and network geometries on methyl orange (MeO) decolorization and cyanide photo-oxidation under UV light irradiation was investigated. The photocatalytic

activity of different samples was estimated via MeO and cyanide degradation. Decolorization of MeO by UV irradiation in the presence of TiO_2 was verified by UV-Vis concentration measurements of the azo dye organic pollutant. The remaining concentration of cyanide was analyzed by the titration method. Catalysts were characterized by XRD, SEM, and BET and each was compared for their catalytic behavior.

2. Materials and Methods

Titanium tetraisopropoxide (TTIP), hydrochloric acid (HCl), 2-propanol, MeO, potassium cyanide (KCN), ethylenediaminetetraacetic acid (EDTA), and P25 Degussa were purchased from MERCK manufacturer. Distilled water, cellulose fibers, and ceramic templates were obtained from local sources.

2.1 Coprecipitation

Distilled water (85 mL), conc. HCl (6 mL), and 2-propanol (6 mL) were mixed and stirred together at room temperature. After thorough mixing, titanium isopropoxide (5 mL) was gradually added to the solution by a pipette. When the solution became clear, its temperature was slowly elevated to 60 °C by immersing its container into a water bath of controlled temperature. The substrates (cellulose fiber or ceramic templates) were then dipped in to the solution and left overnight to allow precipitation of a TiO_2 layer. The sample was then washed with deionized water and dried. The sample was then calcined at 450 °C for 2 h.

Figure 1(a) shows molecular structure of cellulose fiber describing hollow pores which could be employed for fabrication of fibers. Cotton fiber has more than 90% cellulose which by being heated at over 370 °C burns fast (Ref 17). XRD pattern of the ceramic templates employed for manufacture of film or network-shaped samples is represented in Fig. 1(b). Ceramic template is SiC with pore size of 20 PPI, surface area of 2.0×10^4 cm^2 g^{-1}, and open porosity of 85-90%.

2.2 TiO_2 Characterization

X-ray diffractometer (Spectro Xepos, Germany) with Cu K_α radiation was used to determine the XRD patterns of the samples. SEM (Mira 3-XMU; Tescan, Czech Republic) was used for morphological investigation of the samples. Specific surface area of the produced samples was measured by using a Brunauer-Emmett-Teller (BET) surface analyzer (Belsorp mini II; Bel, Japan).

2.3 Photocatalytic Degradation

2.3.1 Methyl Orange. Catalytic activity of the samples was estimated from color degradation of the MeO aqueous solution (50 mL MeO with 5 mg L^{-1} initial concentration). Before irradiation with UV light, the aqueous solution which contained TiO_2 catalyst was continuously stirred for 1 h in full darkness to achieve adsorption-desorption equilibrium. UV irradiation from two 6 W lamp (Philips, China) was then applied to the catalyst containing solution. The distance between the surface of the solution and the light source was 10 cm. Samples were then taken out for analysis, every 30 min.

Solution concentration was determined by UV-Vis spectrophotometer (6705; Jenway, UK). The maximum absorption wavelength registered of MeO was 462 nm.

The efficiency of degradation (η%) was calculated from Eq 1 (Ref 8):

$$\eta\% = \left(\frac{C_0 - C}{C_0}\right) \times 100, \qquad \text{(Eq 1)}$$

where C_0 and C are initial and time-dependant concentrations of the dye, respectively.

2.3.2 Cyanide. Sample solution of cyanide was prepared by dissolving KCN into deionized water (100 mg L^{-1}). Photocatalytic experiments were performed with pH = 10, constant temperature (25 °C), and contact time of 0-180 min in the presence of EDTA (100 mg L^{-1}).

After the equilibration period (60 min in the dark), the UV-lamps (two 6 W lamps, Philips, China) were turned on. The remaining concentration of cyanide was analyzed by 4500-CN D. Titrimetric Method according to Standard Methods for the Examination of Water and Wastewater. Then residual cyanide concentration was calculated using following equation (Ref 18):

$$\frac{\text{mg } CN^-}{\text{L}} = \frac{(A - B) \times 1000}{\text{mL original sample}} \times \frac{250}{\text{mL portion used}}, \qquad \text{(Eq 2)}$$

where A and B is volume (mL) of standard $AgNO_3$ of sample and of blank, respectively.

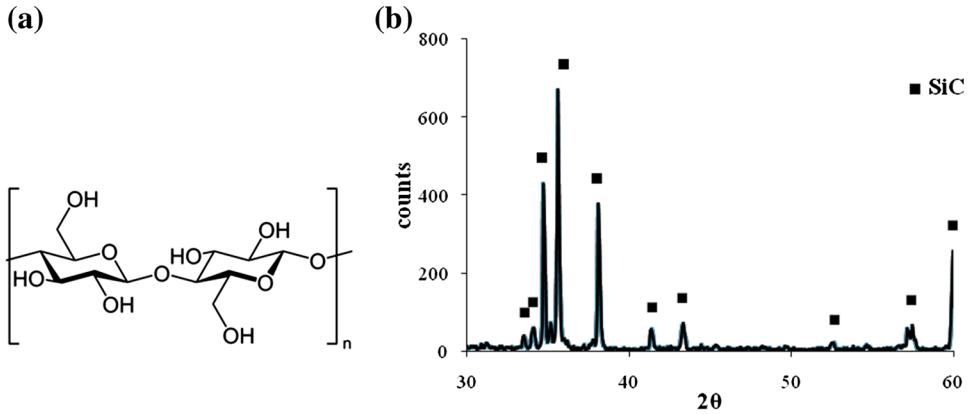

Fig. 1 (a) Molecular structure of cellulose fiber and (b) XRD pattern of the ceramic templates

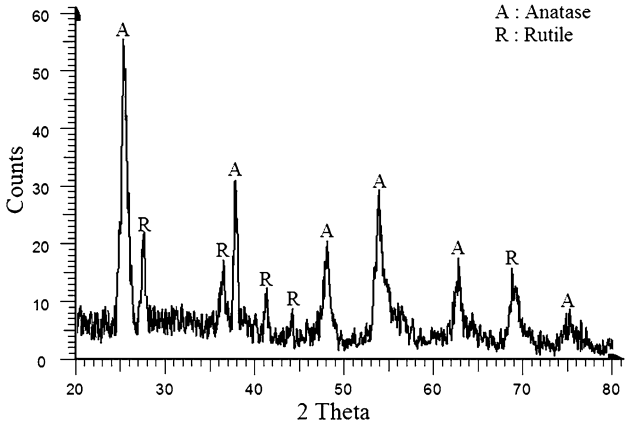

Fig. 2 XRD pattern of TiO_2 powder calcined at 450 °C for 2 h

3. Results and Discussion

In Fig. 2, XRD pattern of TiO_2 is shown. However, this Spectrum belongs to all TiO_2 geometries that have been calcined at 450 °C for 2 h. Based on peaks of this pattern, anatase and rutile are the only phases present in the sample. Using the Scherer equation, the average crystallite sizes of anatase and rutile were estimated to be 19 and 21 nm, respectively.

The fraction of the crystalline phases was determined by integrating the relative intensities of the anatase (101) ($2\theta = 25.4°$) and the rutile (110) ($2\theta = 27.5°$) peaks (Ref 17):

$$W_A = \frac{1}{1 + 1.26\frac{I_R}{I_A}}, \quad \text{(Eq 3)}$$

where W_A is the weight fraction of the anatase and I_A and I_R represent the integrated intensities of the anatase (101) and the rutile (110) peaks, respectively. From Eq 3, the fraction of the anatase in the produced samples was 0.73. This value is related to the samples being calcined at 450 °C. This temperature was selected to ensure that all of the cotton fibers were removed during the calcination process.

SEM images of TiO_2 samples produced in this research are shown in Fig. 3 and 4. Particles shown in Fig. 3(a) have near-spherical agglomerated shape in the size range of 20-40 nm. TiO_2 microfibers shown in Fig. 3(b) are 30 μm long hollow cylinders having 0.5-1 μm diameters. They were produced by template-coating and removal of the cellulose base by subsequent heat treatment. The tubes have open endings. Energy dispersive x-ray (EDS) analysis of the fibers shown in Fig. 3(c) indicated the presence of Ti and O in the annealed samples. Therefore, calcination at 450 °C for 2 h led to the removal of all cellulose of template. SEM image of the TiO_2 film is shown in Fig. 4(a). As can be observed, particles in the size range of 20-60 nm covered the surface of the substrate relatively uniformly. From Fig. 4(b), the thickness of the film is 10-12 μm. Figure 4(c) shows an EDS diagram of film sample; according to the substrate SiC, only two elements oxygen and titanium on the surface are detected.

Figure 5(a) illustrates network-shaped substrate. The TiO_2 particles deposited on wall of the substrate are highlighted in Fig. 5(b). This deposit layer has a thickness of less than 10 μm (Fig. 5c). By studying the EDS diagram in Fig. 5(d), only the presence of oxygen and titanium is confirmed.

The specific surface areas, pore volume, and average particle size of all photocatalysts which were used in this research are also listed in Table 1. The average particle size was estimated by assuming all the particles to have same spherical shape and size (Ref 19). The particle size, D, is given by Eq 4,

$$D = \frac{6000}{S_{BET} \times \rho}, \quad \text{(Eq 4)}$$

where S_{BET} is the BET-specific surface area and ρ is the true density (ρ for titania is 4.2 g mL^{-1}) (Ref 19).

It can be seen that the surface area of TiO_2 powder is larger than other samples. In the coated samples (film and network), due to the agglomeration of the particles, the surface area decreased and average particle size increased. In fact, the surface area of the catalyst is minimized since the coating layer has a lower porosity. Due to the accumulation of fibers and closure of some of them, the surface area of the fiber sample is greatly reduced.

For a general first-order reaction, the equation relating the k_{app} is the apparent-first-order reaction rate constant (min^{-1}), C_0 is the initial concentration of MeO dye in the bulk solution (mg L^{-1}), and t is the reaction time (min) is given as (Ref 20)

$$r = -\frac{dC}{dt} = k_{app}C \quad \text{(Eq 5)}$$

$$\ln\left(\frac{C_0}{C}\right) = k_{app}t. \quad \text{(Eq 6)}$$

Figure 6 compares the (C/C_0) ratio against time for different catalysts with and without UV irradiation. A pseudo-first-order kinetic model (Eq 6) was applied to compare the degradation performance of different catalysts and no UV tests. MeO degradation in the presence of powder without UV irradiation was about 75% lower in comparison with the removal with UV light. P25 and synthesized powder reduced the MeO concentration faster than other samples.

The plot of $\ln(C_0/C)$ versus time was close to linear for all experiments (Fig. 7). Same initial concentrations (5 mg L^{-1}) of MeO were used to obtain data of Fig. 7. Degradation rate constant (k) of the MeO dye in Table 2 was obtained by regression analysis of the data given in Fig. 7. Effect of TiO_2 geometry on efficiency of the MeO degradation is shown in Fig. 8. Examining Fig. 6, 7, and 8, the powdery sample yields the highest degradation. Its use is not, however, desirable because its collection after utilization is a total mess (Ref 1).

Release degree (RD) of the prepared geometries in pure water was determined by UV-Vis spectrophotometer. Powdery catalyst with 100% RD moves with the solution and cannot be removed from the reaction environment easily. Fiber, film, and network structures have RD of 48, 6, and 9%, respectively. Network geometry is hence the most suitable TiO_2 catalyst shape. It has all the advantages of production simplicity, environmental stability, and high catalytic performance.

The mechanism of cyanide removal is based on the absorption of light energy, by the semiconductor particles, which must be of a wavelength sufficient to exceed the band gap energy of the semiconductor, which produces electron-hole pairs (e^--h^+) (Ref 21). From the reaction of cyanide ion with positive hole, CN^- is oxidized to OCN^-, while oxygen is photoreduced to hydrogen peroxide by photogenerated elec-

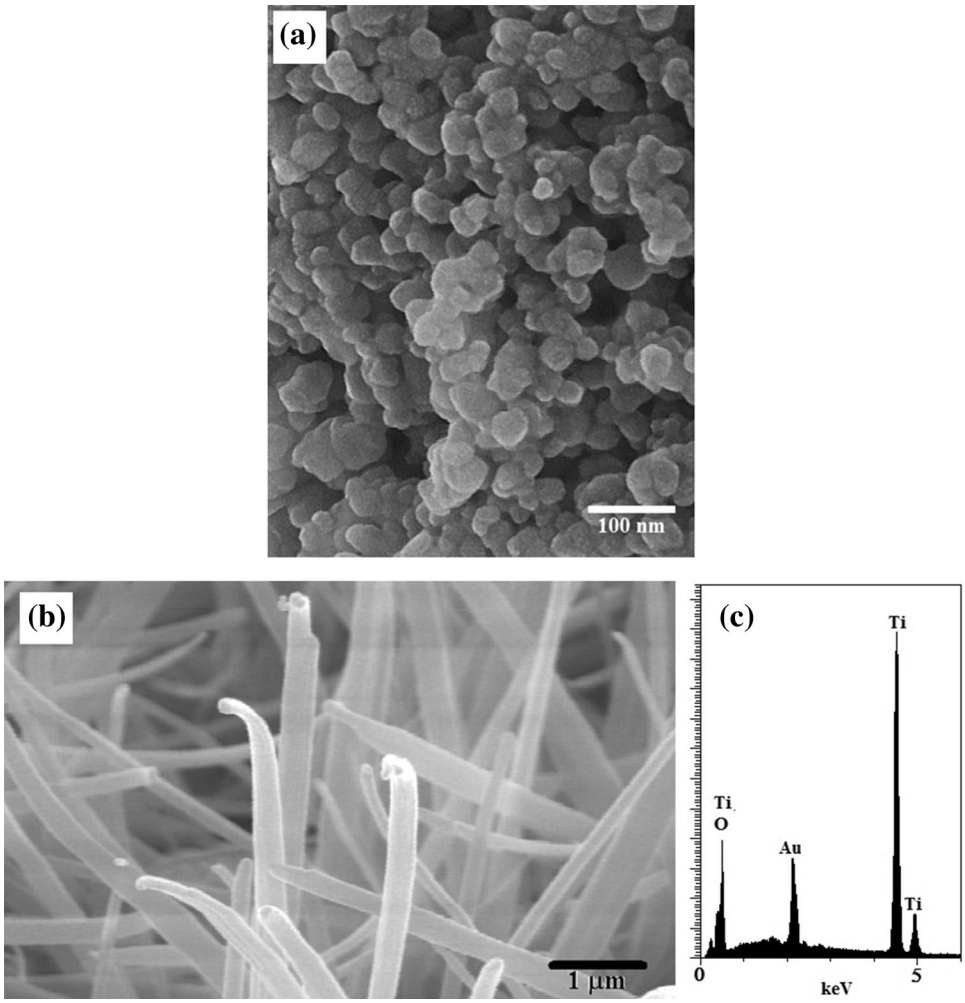

Fig. 3 SEM images of TiO_2 (a) powder and (b) fiber samples and (c) EDS diagram of fibers

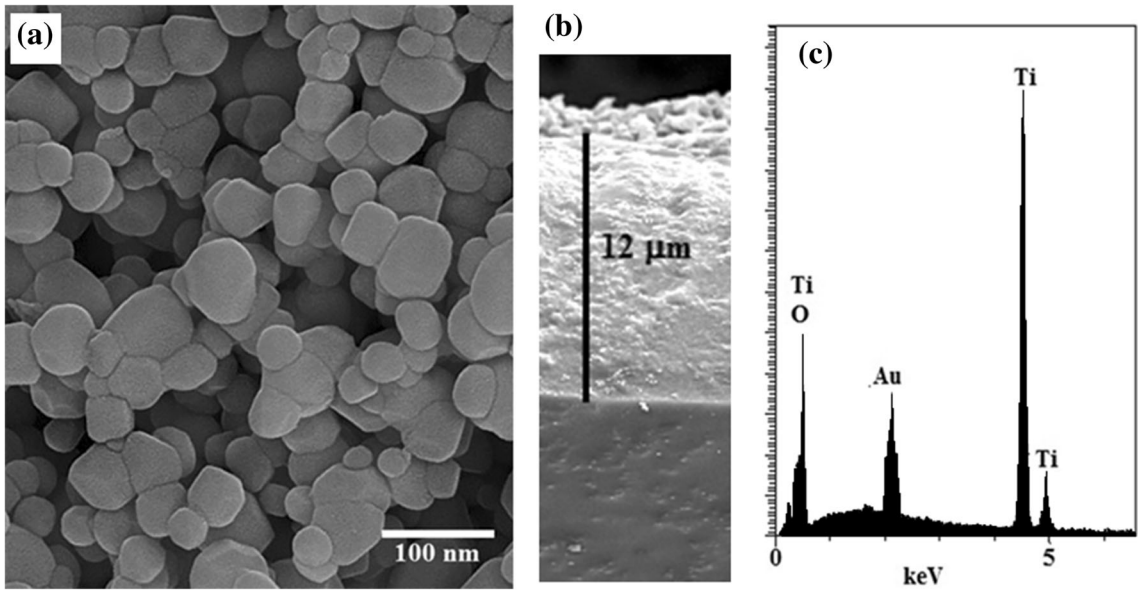

Fig. 4 TiO_2 film: (a) SEM image, (b) cross-section image, and (c) EDS diagram

trons in the conduction band of photocatalysts. Thus, the process for removal of CN^- can be represented as follows (Ref 22):

$$TiO_2 + 2h\nu = TiO_2(2h^+ + 2e^-) \quad \text{(Eq 7)}$$

$$\frac{1}{2}O_2 + 2e^- + H_2O = 2OH^- \quad \text{(Eq 8)}$$

$$2OH^- + 2h^+ = 2OH^{\cdot} \quad \text{(Eq 9)}$$

$$CN^- + 2OH^{\cdot} = OCN^- + H_2O \quad \text{(Eq 10)}$$

$$2OCN^- + O_2 = 2CO_2 + N_2. \quad \text{(Eq 11)}$$

The initial concentration of cyanide employed in this study was low, and the adsorption kinetics can be described adequately by a simplified first-order rate equation:

$$\ln[C_0/C_t] = kt, \quad \text{(Eq 12)}$$

where C_0 and C_t are the cyanide concentration at initial and at time t, respectively. k is the first-order rate constant and t is the reaction time (Ref 21).

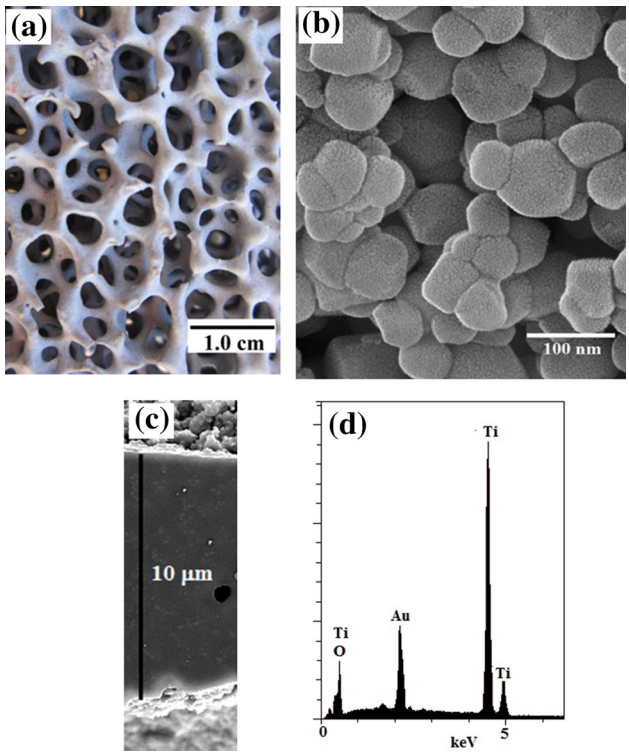

Fig. 5 TiO_2 network sample: (a) shape of substrate, (b) SEM image, (c) cross-section image, and (d) EDS diagram

The influence of photocatalyst geometry on the efficiency of cyanide degradation in the UV/TiO_2 system is presented in Fig. 9. The powder sample, due to the greater surface area, has higher removal efficiency. Immobilization and the support material have important influence on the photocatalyst activity. Due to the significant advantages of immobilized photocatalyst, network geometry does properly remove cyanide. It can cause more contact time between the cyanide solution and photocatalyst.

Figure 10 shows the plot of $\ln[C_0/C_t]$ versus of t for the removal of cyanide by TiO_2 samples. Rate constants (min^{-1}) and linear regression coefficients (R^2) are summarized in Table 2. The results indicate that photo-degradation in the presence of TiO_2 samples kinetics were satisfactorily fit to a first-order rate law. The rate constants of fiber and film geometry are around 0.0019 and 0.0040 min^{-1}, while the rate constant of network geometry is 0.0046 min^{-1}. As a result, the

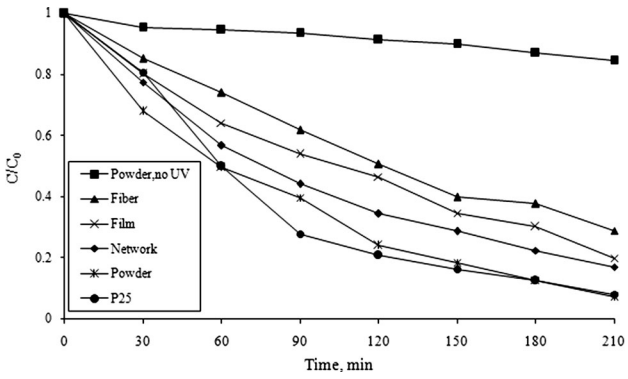

Fig. 6 MeO degradation dependence on geometry of the TiO_2

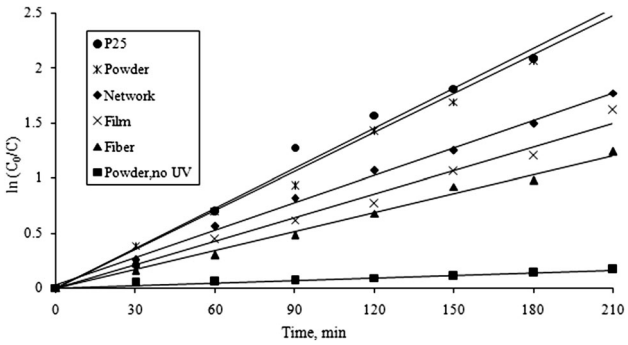

Fig. 7 First-order kinetic plots of the MeO photo-degradation in the presence of different catalysts

Table 1 Surface area for various geometries

	P25	TiO_2 powder	TiO_2 film	TiO_2 fiber	TiO_2 network
S_{BET}, $m^2\ g^{-1}$	56(a)	68	58	48	60
Pore volume, $cm^3\ g^{-1}$	0.25	0.37	0.29	0.22	0.29
Particle size(b), nm	26	21	25	30	24

(a) See Militky (Ref 17); (b) S_{BET} method

Table 2 Kinetic parameters for MeO degradation and removal of cyanide on samples

Sample	Methyl orange		Cyanide	
	K, 1/min	R^2	K, 1/min	R^2
P25	0.0122	0.985	0.0062	0.972
Powder	0.0118	0.989	0.0055	0.979
Network	0.0083	0.997	0.0046	0.978
Film	0.0071	0.985	0.0040	0.985
Fiber	0.0057	0.991	0.0019	0.966
Powder, no UV	0.0008	0.957	…	…

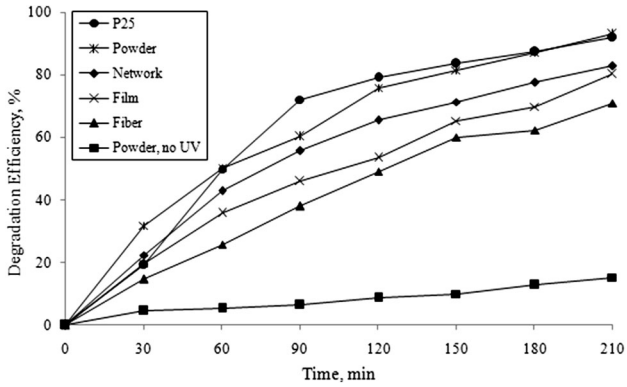

Fig. 8 Comparison of MeO degradation for different catalysts and no UV irradiation

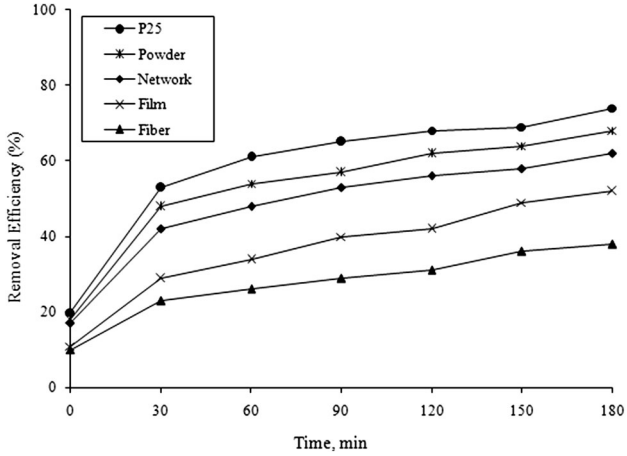

Fig. 9 Effect of geometry of TiO_2 on the removal of cyanide under UV light

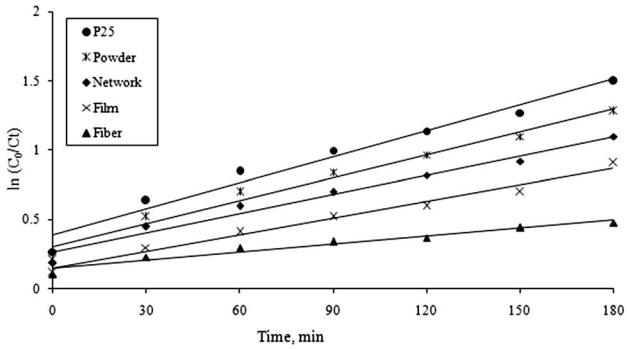

Fig. 10 First-order kinetic model for cyanide removal by TiO_2 samples

rate constant at the same initial condition is powder > network > film > fiber geometry.

4. Conclusions

In this work, four geometries of TiO_2 (powder, fiber, film, and network) were produced by precipitation from a synthesized raffinate. Morphologies of the samples were determined from their SEM images. Their photocatalytic properties were determined from MeO degradation data obtained from color change and solution composition alteration. Also, the photooxidation of cyanide by the different geometries of TiO_2 was compared. The network geometry was introduced as the most desirable TiO_2 catalyst shape.

References

1. H. Koohestani, and S.K. Sadrnezhaad, The influence of structures on the TiO_2 photocatalytic properties, *5th International Conference on Nanostructures (ICNS5)*, 2014, Mehregan Ghalam, Kish Island
2. M.J. Benotti et al., Evaluation of a Photocatalytic Reactor Membrane Pilot System for the Removal of Pharmaceuticals and Endocrine Disrupting Compounds from Water, *Water Res.*, 2009, **43**(6), p 1513–1522
3. S. Ray et al., Removal of Nitrate and COD from Wastewater Using Denitrification Process: Kinetic, Optimization, Statistical Studies, *Clean Technol. Environ. Policy*, 2014, **16**(2), p 291–301
4. R. Salazar, E. Brillas, and I. Sirés, Finding the Best Fe^{2+}/Cu^{2+} Combination for the Solar Photoelectro-Fenton Treatment of Simulated Wastewater Containing the Industrial Textile Dye Disperse Blue 3, *Appl. Catal. B*, 2012, **115**, p 107–116
5. M.N. Chong et al., Recent Developments in Photocatalytic Water Treatment Technology: A Review, *Water Res.*, 2010, **44**(10), p 2997–3027
6. Y. Okour et al., Preparation and Characterisation of Titanium Dioxide (TiO_2) and Thiourea-Doped Titanate Nanotubes Prepared from Wastewater Flocculated Sludge, *Bioresour. Technol.* , 2010, **101**(5), p 1453–1458
7. C.M. Teh and A.R. Mohamed, Roles of Titanium Dioxide and Ion-Doped Titanium Dioxide on Photocatalytic Degradation Of Organic Pollutants (Phenolic Compounds and Dyes) in Aqueous Solutions: A Review, *J. Alloys Compd.*, 2011, **509**(5), p 1648–1660
8. N. Laoufi, D. Tassalit, and F. Bentahar, The Degradation of Phenol in Water Solution by TiO_2 Photocatalysis in a Helical Reactor, *Glob. NEST J.*, 2008, **10**(3), p 404–418
9. A.H. Jawad, A.F. Alkarkhi, and N.S.A. Mubarak, Photocatalytic Decolorization of Methylene Blue by an Immobilized TiO_2 Film Under Visible Light Irradiation: Optimization Using Response Surface Methodology (RSM), *Desalin. Water Treat.*, 2014(ahead-of-print), p 1–12
10. T. An et al., Photocatalytic Degradation Kinetics and Mechanism of Antivirus Drug-Lamivudine in TiO_2 Dispersion, *J. Hazard. Mater.*, 2011, **197**, p 229–236

11. S. Papageorgiou et al., Alginate Fibers as Photocatalyst Immobilizing Agents Applied in Hybrid Photocatalytic/Ultrafiltration Water Treatment Processes, *Water Res.*, 2012, **46**(6), p 1858–1872
12. A.Y. Shan, T.I.M. Ghazi, and S.A. Rashid, Immobilisation of Titanium Dioxide onto Supporting Materials in Heterogeneous Photocatalysis: A Review, *Appl. Catal. A*, 2010, **389**(1), p 1–8
13. E. Khaksar, M.S. Afarani, and A. Samimi, In Situ Solvothermal Crystallization of TiO_2 Nanostructure on Alumina Granules for Photocatalytic Wastewater Treatment, *J. Mater. Eng. Perform.*, 2014, **23**(1), p 92–100
14. L. Lim, R. Lynch, and S.-I. In, Comparison of Simple and Economical Photocatalyst Immobilisation Procedures, *Appl. Catal. A*, 2009, **365**(2), p 214–221
15. K. Nakata and A. Fujishima, TiO_2 Photocatalysis: Design and Applications, *J. Photochem. Photobiol., C*, 2012, **13**(3), p 169–189
16. X. Zhang, et al., "Construction of Self-Supported Three-Dimensional TiO_2 Sheeted Networks with Enhanced Photocatalytic Activity," Scientific Reports, 2013, vol. 3
17. J. Militky, *Structure and Properties of Cotton Fiber: A Literature Review*, 2009, Dr Muhammad Mushtaq Mangat
18. E.W. Rice, and A.P.H. Association, *Standard Methods for the Examination of Water and Wastewater*, 2012, American Public Health Association, Washington, DC
19. K.J.A. Raj and B. Viswanathan, Effect of Surface Area, Pore Volume and Particle Size of P25 Titania on the Phase Transformation of Anatase to Rutile, *Indian J. Chem. A*, 2009, **48**, p 1378
20. C. Wang et al., Reaction Kinetics of Photocatalytic Degradation of Sulfosalicylic Acid Using TiO_2 Microspheres, *J. Hazard. Mater.*, 2009, **163**(2), p 1101–1106
21. E.M. Rodríguez et al., Mechanism Considerations for Photocatalytic Oxidation, Ozonation and Photocatalytic Ozonation of Some Pharmaceutical Compounds in Water, *J. Environ. Manag.*, 2013, **127**, p 114–124
22. I. Ibrahim, A. Ismail, and R. Mohamed, Degradation of Free Cyanide by Photocatalytic Oxidation, *Eur. J. Miner. Process. Environ. Prot.*, 2003, **3**(3), p 281–290